8. Smith, R. C. & Baker, K. S. in *The Role of Solar Ultraviolet Radiation in Marine Ecosystems* (ed. Calkins, J.) 509–537 (Plenum, New York, 1982).
9. Neale, P. J., Cullen, J. J. & Davis, R. F. Inhibition of marine photosynthesis by ultraviolet radiation: Variable sensitivity of phytoplankton in the Weddell-Scotia Confluence during the austral spring. *Limnol. Oceanogr.* (in the press).
10. Behrenfeld, M. J., Chapman, J. W., Hardy, J. T. & Lee, H. II Is there a common response to ultraviolet-b radiation by marine phytoplankton. *Mar. Ecol. Prog. Ser.* **102,** 59–68 (1993).
11. Cullen, J. J., Neale, P. J. & Lesser, M. P. Biological weighting function for the inhibition of phytoplankton photosynthesis by ultraviolet radiation. *Science* **258,** 646–650 (1992).
12. Boucher, N. P. & Prézelin, B. B. Spectral modeling of UV inhibition of *in situ* Antarctic primary production using a field derived biological weighting function. *Photochem. Photobiol.* **64,** 407–418 (1996).
13. Veth, C. The evolution of the upper water layer in the marginal ice zone, austral spring 1988, Scotia-Weddell Sea. *J. Mar. Syst.* **2,** 451–464 (1991).
14. Nelson, D. M. & Smith, W. O. Jr Sverdrup revisited: Critical depths, maximum chlorophyll levels, and the control of Southern Ocean productivity by the irradiance-mixing regime. *Limnol. Oceanogr.* **36,** 1650–1661 (1991).
15. Cullen, J. J. & Lesser, M. P. Inhibition of photosynthesis by ultraviolet radiation as a function of dose and dosage rate: Results for a marine diatom. *Mar. Biol.* **111,** 183–190 (1991).
16. Franks, P. J. S. & Marra, J. A simple new formulation for phytoplankton photoresponse and an application in a wind-driven mixed-layer model. *Mar. Ecol. Prog. Ser.* **111,** 145–153 (1994).
17. Yamazaki, H. & Kamykowski, D. The vertical trajectories of motile phytoplankton in a wind-mixed water column. *Deep-Sea Res.* **38,** 219–241 (1991).
18. Anis, A. & Moum, J. N. Surface wave-turbulence interactions: scaling $\epsilon(z)$ near the sea surface. *J. Phys. Oceanogr.* **25,** 2025–2045 (1995).
19. Prézelin, B. B., Boucher, N. P. & Smith, R. C. in *Ultraviolet Radiation in Antarctica: Measurements and Biological Effects* (eds Weiler, C. S. & Penhale, P. A.) 159–186 (Am. Geophys. Union, Washington DC, 1994).
20. Helbling, E. W., Villafañe, V., Ferrario, M. & Holm-Hansen, O. Impact of natural ultraviolet radiation on rates of photosynthesis and on specific marine phytoplankton species. *Mar. Ecol. Prog. Ser.* **80,** 89–100 (1992).
21. Zepp, R. G. & Cline, D. M. Rates of direct photolysis in aquatic environment. *Environ. Sci. Technol.* **11,** 359–366 (1977).
22. Murray, A. G. & Jackson, G. A. Viral dynamics II: a model of the interaction of ultraviolet light and mixing processes on virus survival in seawater. *Mar. Ecol. Prog. Ser.* **102,** 105–114 (1993).
23. Vincent, W. F. & Roy, S. Solar ultraviolet-B radiation and aquatic primary production: damage, protection and recovery. *Environ. Rev.* **1,** 1–12 (1993).
24. Morel, A. Available, usable, and stored radiant energy in relation to marine photosynthesis. *Deep-Sea Res.* **25,** 673–688 (1978).
25. Cullen, J. J. & Neale, P. J. in *The Effects of Ozone Depletion on Aquatic Ecosystems* (ed. Häder, D.-P.) 97–118 (Landes, Austin, 1997).
26. Gregg, W. W. & Carder, K. L. A simple spectral solar irradiance model for cloudless maritime atmospheres. *Limnol. Oceanogr.* **35,** 1657–1675 (1990).
27. Davis, R. F., Lazin, G., Bartlett, J., Ciotti, A. & Stabeno, P. Remote sensing of a pigment patch in the southeastern Bering Sea. *Proc. SPIE* **2963,** 654–657 (1997).
28. Prieur, L. & Sathyendranath, S. An optical classification of coastal and oceanic waters based on the specific absorption curves of phytoplankton pigments, dissolved organic matter, and other particulate materials. *Limnol. Oceanogr.* **26,** 671–689 (1981).
29. Sakshaug, E., Johnsen, G., Andersen, K. & Vernet, M. Modeling of light-dependent algal photosynthesis and growth: experiments with Barents Sea diatoms *Thalassiosira nordenskioeldii* and *Chaetoceros furcellatus*. *Deep-Sea Res.* **38,** 415–430 (1991).
30. Denman, K. L. & Gargett, A. E. Time and space scales of vertical mixing and advection of phytoplankton in the upper ocean. *Limnol. Oceanogr.* **28,** 801–815 (1983).

Acknowledgements. We thank members of the science team, officers and crew of the *Nathaniel B. Palmer* cruise NBP93-6 for assistance, W. Helbling, C. Gallegos, J. Christian, M. Lewis and B. Nieke for comments, D. Kelley for discussions of vertical mixing, M. Lesser for use of his spectroradiometers and P. Franks for providing his version of the mixing model. This work was supported by the NSF Office of Polar Programs, NSERC, NASA, and ONR Ocean Optics.

Correspondence and requests for materials should be addressed to J.J.C. (e-mail: John.Cullen@Dal.CA).

Increased polar stratospheric ozone losses and delayed eventual recovery owing to increasing greenhouse-gas concentrations

Drew T. Shindell, David Rind & Patrick Lonergan

NASA Goddard Institute for Space Studies and Center for Climate Systems Research, Columbia University, 2880 Broadway, New York, New York 10025, USA

The chemical reactions responsible for stratospheric ozone depletion are extremely sensitive to temperature[1]. Greenhouse gases warm the Earth's surface but cool the stratosphere radiatively[2–5] and therefore affect ozone depletion. Here we investigate the interplay between projected future emissions of greenhouse gases and levels of ozone-depleting halogen species using a global climate model that incorporates simplified ozone-depletion chemistry. Temperature and wind changes induced by the increasing greenhouse-gas concentrations alter planetary-wave propagation in our model, reducing the frequency of sudden stratospheric warmings in the Northern Hemisphere[4]. This results in a more stable Arctic polar vortex, with significantly colder temperatures in the lower stratosphere and concomitantly increased ozone depletion. Increased concentrations of greenhouse gases might therefore be at least partly responsible for the very large Arctic ozone losses observed in recent winters[6–9]. Arctic losses reach a maximum in the decade 2010 to 2019 in our model, roughly a decade after the maximum in stratospheric chlorine abundance. The mean losses are about the same as those over the Antarctic during the early 1990s, with geographically localized losses of up to two-thirds of the Arctic ozone column in the worst years. The severity and the duration of the Antarctic ozone hole are also predicted to increase because of greenhouse-gas-induced stratospheric cooling over the coming decades.

Parametrized chemistry was included interactively in the Goddard Institute for Space Studies (GISS) Global Climate/Middle Atmosphere Model (GCMAM)[10], a primitive equation model including parametrized gravity waves. This model has $8° \times 10°$ resolution (latitude × longitude), with 23 vertical layers extending from the surface to 85 km. Mountain wave drag was reduced globally to one-quarter its usual value[11] to allow realistic simulation of Southern Hemisphere polar lower-stratospheric temperatures, which were otherwise too warm. Modelled ozone transport was fixed at climatological values. This includes only zonal mean motions, so that we may underestimate the amount of chemical processing by longitudinally asymmetric motion of air across low-temperature regions. Ozone transport changes induced by increasing greenhouse gases were calculated non-interactively. We performed a control run without greenhouse gas forcing, and a run with forcings (Fig. 1), each including the chlorine loading trend[1,12,13]. Both began in 1959, allowing time for removal of any influence of initial conditions, and continued to the end of 2070. The atmosphere was coupled to a mixed-layer ocean with specified

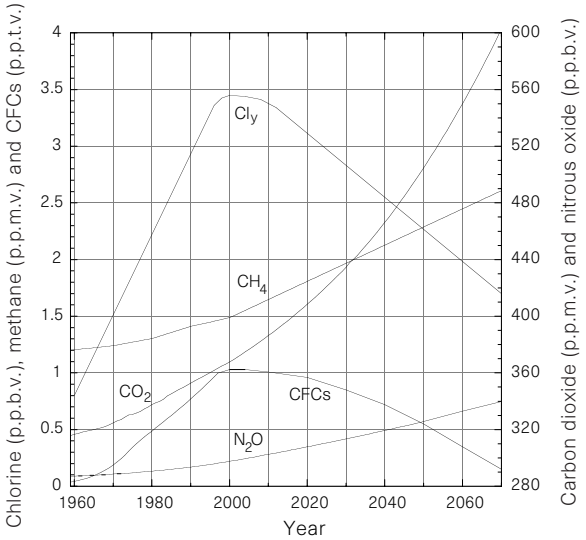

Figure 1 Emission trends for CO_2, N_2O, CH_4, CFCs and chlorine (Cl*y*) used as input to the model runs. Projected lower stratospheric chlorine loading (independent of height or latitude) is based on the trend derived from the 1992 Copenhagen revisions to the 1987 Montreal Protocol on Substances that Deplete the Ozone Layer[1], normalized slightly upwards and decreasing more slowly in the future to match recent observations[12,13,30]. Greenhouse-gas emissions are based on observations to the end of 1984, and subsequently are similar to, though for carbon dioxide slightly lower than, the 1992 International Panel on Climate Change (IPCC) preferred scenario IS92a[25]. The exception is CFCs, for which a steady reduction after 2000 has been assumed, consistent with their expected phase-out and with the chlorine loading scenario.

ocean heat transports and diffusion through the base of the mixed layer, allowing sea surface temperatures to respond to greenhouse forcings[4].

A simple, but physically realistic parametrization of the heterogenous chemistry responsible for polar ozone depletion was used[11,14]. Computational resources prohibit the use of more complex chemistry. Briefly, chlorine activation takes place whenever temperatures fall below 195 K, a rough threshold for formation of polar stratospheric cloud or supercooled sulphate aerosol, as observations and detailed photochemical calculations show rapid activation below this temperature regardless of phase and composition details of heterogeneous surfaces[15,16]. Ozone depletion takes place at each location with active chlorine and sunlight according to photochemistry and temperature[17]. An additional contribution of 15% from bromine chemistry is also included. This parametrization reproduces quite well observed global chlorine monoxide abundances[18] and polar ozone losses[11], and has been used in previous studies of ozone response to climate change[14]. Other models using crude heterogeneous chemistry parametrizations have also obtained reasonable results for global-scale ozone loss[19–21]. We note that should massive denitrification occur in the Arctic, ozone loss could be extended even beyond that modelled here.

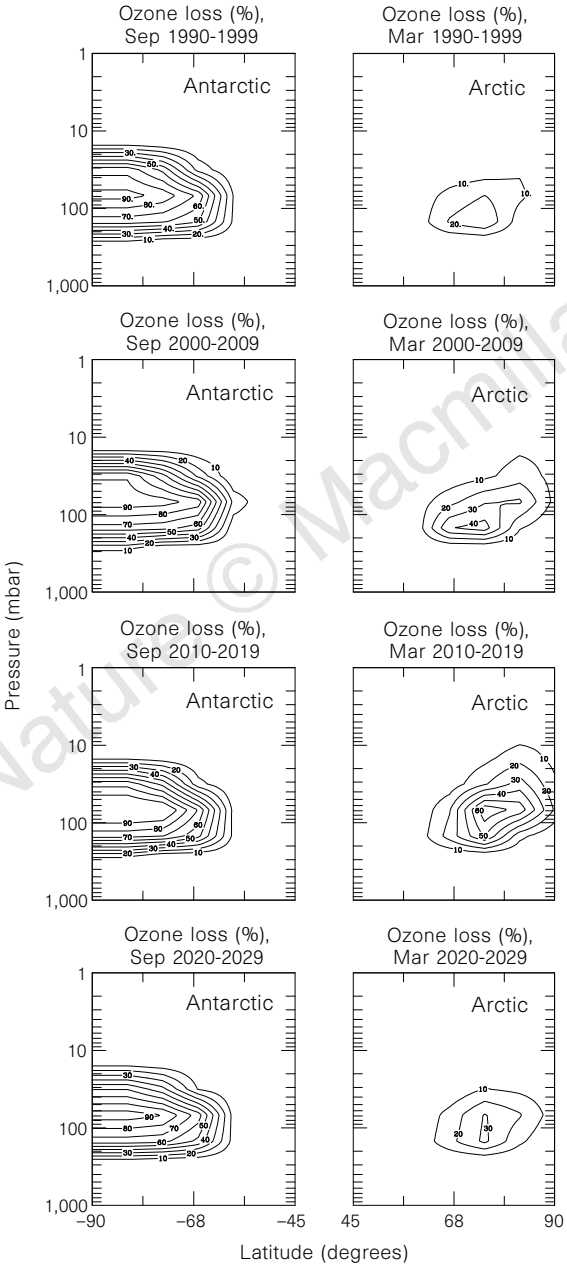

Figure 2 Decadally averaged vertical profiles of zonal mean ozone losses during September for the Southern Hemisphere and during March for the Northern Hemisphere. Values are percentage depletion with respect to pre-1980 observed climatological ozone.

Radiative cooling by increasing greenhouse gases by itself causes area-weighted temperature decreases of ~1–2 K poleward of 70° from altitudes of 200 to 50 mbar during 2010–19 in the winter in both hemispheres, relative to the control run. In the Northern Hemisphere, the reduced frequency of stratospheric warmings adds to the radiative cooling, resulting in total temperature decreases within the enhanced Arctic vortex of 5–7 K during December and January. Large ozone losses in February and March exert a sizeable positive feedback, so that modelled temperatures are 8–10 K colder in the greenhouse run owing to combined radiative, dynamical and chemical influences.

In the Southern Hemisphere, the radiative cooling and the resulting positive feedback from increased chemical ozone loss lead to more persistent extremely cold temperatures. Although an Antarctic ozone hole occurs in the control run, November and December are 4 K colder during 2010–19 in the run with increasing greenhouse gases, prolonging the duration of the ozone hole. (The 1990s Antarctic ozone hole itself induced lower-stratospheric cooling of ~6 K in October, and ~8 K in November in the model[11], in good agreement with observations.) Total modelled cooling relative to pre-ozone-hole conditions in the 2010s is ~7 K in October, and ~12 K in November, similar to the Arctic values.

Figure 2 shows that Arctic ozone losses are greatest in the 2010s, while during the late 1990s and early 2000s they are similar in percentage to Antarctic losses observed in the late 1980s. Without climate forcing, average ozone destruction would only change within the model as a result of changes in chlorine amounts. Chlorine abundance in the 2010s is similar to 1990s levels, so that the much greater mean Arctic ozone loss in the 2010s displays the distinct signature of stratospheric cooling induced by increasing greenhouse gases. Greenhouse-gas-induced lower-stratospheric cooling also causes the Antarctic ozone hole to expand vertically and horizontally relative to its current state, as seen in equilibrium doubled CO_2 experiments[11,19]. As ozone depletion is already very large, additional destruction over that seen in the current decade is fairly small. Recovery of ozone to early 1980s levels does not take place until roughly 2050.

Antarctic ozone depletion is up to 50–60% of the column during 2010–19, and roughly symmetric around the South Pole (Fig. 3). Though interannual variability remains large, over 50% of the ozone column is also frequently destroyed over a large area of the Arctic. The total amount of ozone destroyed in the Arctic during this decade is ~85% of Antarctic destruction during the same decade. Over Greenland and Northern Europe however, more ozone is destroyed than anywhere within the Antarctic ozone hole.

In Fig. 4 we compare observed and modelled Antarctic and Arctic ozone column minima. Within the large variability, the model reproduces well the decreasing values seen in the 1990s in both hemispheres. The most severe Arctic depletions are seen during 2006–21, when column minima drop below 150 Dobson units (DU) during four of the coldest, most stable years.

Ozone transport differences between the control and experimental runs were calculated non-interactively[14]. The stronger Arctic polar vortex slows meridional transport across the vortex boundary, leading to a slight ozone build-up outside the vortex, with associated slight ozone decreases within the vortex. Additionally, increased residual circulation brings down more ozone into the highest altitudes where ozone depletion occurs. These effects change ozone amounts by less than 8% at any point during 2010–19; a small value relative to chemical losses. Southern Hemisphere

changes are even smaller. In contrast, altered transports in an equilibrium doubled-CO_2 experiment with the GISS model changed Arctic ozone amounts by more than 25% (ref. 14), so the importance of transport changes is likely to increase significantly towards the middle of the next century.

Whereas climate models are fairly consistent in generating lower-stratospheric radiative cooling in response to increasing greenhouse gases, changes in planetary-wave energy propagation may be much more model-dependent. These experiments show that Arctic ozone loss is extremely sensitive to a reduction in the frequency of sudden stratospheric warmings, agreeing with earlier work demonstrating that the presence, or lack of, mid-winter sudden stratospheric warming is the crucial factor in determining whether an Arctic ozone hole will form under doubled-CO_2 conditions[22,23].

The GISS model generates a large tropical upper-tropospheric warming in response to increasing greenhouse gases: 10 K in the doubled-CO_2 experiments, 3 K during the 2010s in these experiments. This warming increases the latitudinal temperature gradient over the altitude range ~600–100 mbar, causing the lower-stratospheric (300–10 mbar) zonal winds at 40–50° N during December–February to speed up by 9–11 m s^{-1} for doubled CO_2, and 3–5 m s^{-1} during the 2010s in these experiments, relative to the control runs. Faster winds alter the refraction of planetary waves, limiting the ability of wave number two (planetary wave n is the wave with n nodes) to propagate up into the stratosphere[4]. Sudden warmings in our model are typically triggered by a combination of waves one and two, especially major warmings (as has often been observed[24]). The net result is a reduction in the frequency of stratospheric warmings despite an enhancement of wave one. This mechanism therefore depends upon the degree of tropical upper-tropospheric warming due to increased CO_2 generated by a particular model. We note that another GISS model with 31 vertical layers and 4° × 5° resolution produces a similar upper-tropospheric warming, as does the 23-layer model with standard mountain drag, suggesting that this response is not very sensitive to model resolution or mountain drag. Whereas models such as the UK Meteorological Office model generate upper-tropospheric warmings similar to those of the GISS model, others (such as the models of the Geophysical Fluid Dynamics Laboratory or the National Center for Atmospheric Research) do not[25]. The Météo-France group performed an experiment using prescribed temperature changes in response to CO_2 increases as calculated in the Hamburg model, which gave a weaker temperature response than is typical[25]. Though they did not calculate polar ozone loss, they found an increase in the frequency of sudden stratopheric warmings with a doubling of atmospheric carbon dioxide[5].

In support of the GISS model, observations generally agree with the trends seen in our simulations. The winter-time Arctic vortex area with temperatures below 195 K has increased considerably over the past three decades[26], as have winter-time lower-stratospheric zonal winds[27]. Recent Arctic winters have followed the trends in our model, showing large ozone losses and an increasingly stable and

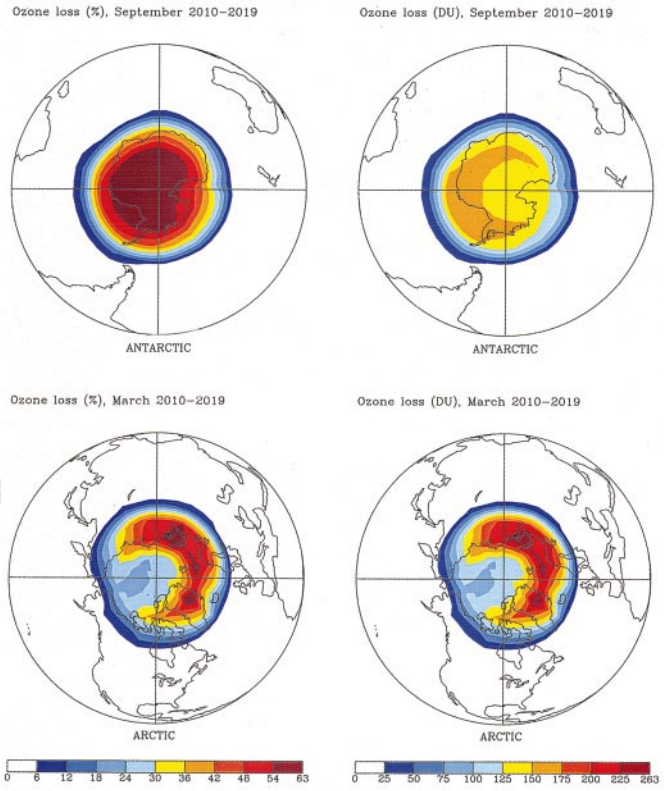

Figure 3 Total column ozone loss averaged over 2010–19, during September for the Southern Hemisphere (top) and March for the Northern Hemisphere (bottom). The left-hand panels show the total ozone column loss in per cent. In the Arctic, despite the enhanced polar vortex, decadal mean loss is very non-symmetric. The GISS GCMAM produces an Aleutian high-pressure region in good agreement with observations, resulting in colder temperatures on average from 90° W through 0° to 90° E. Average ozone losses are therefore greater in that region. As there is more springtime ozone in the Northern Hemisphere than in the Southern Hemisphere, in addition to showing the relative percentage losses, total column loss is also shown in Dobson units (DU; right-hand panels), indicating the absolute number of ozone molecules destroyed.

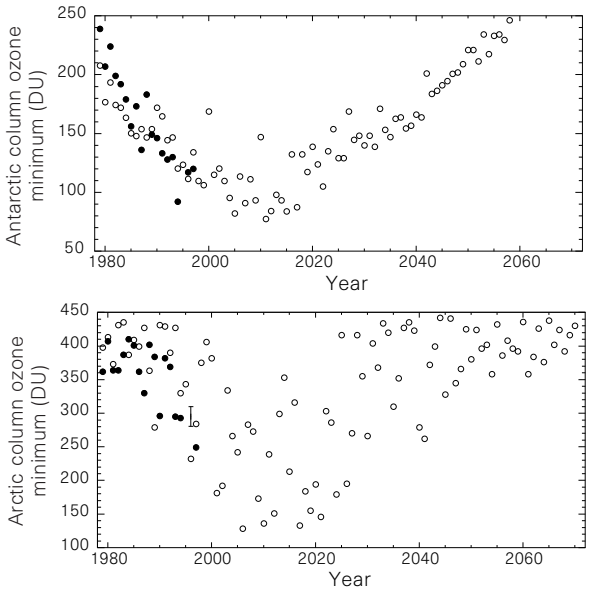

Figure 4 Total column ozone minima in the polar regions during spring. The top panel shows minimum ozone (DU) south of 65° averaged over the last three days of September (except for 1993, for which 23–25 September was used), as seen in TOMS version 7 data (filled circles), and in the model (open circles). Similarly, the bottom panel shows minimum column ozone north of 65°, averaged over the last three days of March, as seen in TOMS data and in the model. Model values do not include intrusions of low-ozone air from lower latitudes into the Arctic, so they tend to be on the high side of observed values. The bar shown for 1996 is an estimate for that year derived from chemical column depletions of 120–160 DU with respect to a climatological mean of 435 DU, calculated based on Halogen Occultation Experiment observations[7].

persistent polar vortex[6–9,28]. In the first eight years of the 1990s, there has been only one Arctic major warming during December–February, as compared with five during the 1980s.

The model results are triggered by changes in the tropopause-region latitudinal temperature gradient. This gradient can be increased by both greenhouse warming and by high-latitude ozone loss (recent trends[26–28] have probably been influenced by both). High-latitude ozone loss provides a positive feedback loop, creating nonlinear dynamical and ozone responses to climate forcing. Observations of the temporal evolution of the tropopause-region latitudinal temperature gradient are therefore crucial. Combined with measurements of the frequency of sudden stratospheric warmings, they may verify our modelled chemistry–climate linkage which creates a severe Arctic ozone hole.

Despite worldwide limits on chlorofluorocarbon (CFC) production implemented after the discovery of the ozone hole over Antarctica[29], uncertainties remain about the exact timing of ozone-hole recovery. Our results suggest that increasing greenhouse gases may worsen the situation, leading to severe ozone depletion over the Arctic, as well as increasing the severity and duration of the Antarctic ozone hole. Furthermore, due to the influence of climate change, the maximum chemical depletion of polar ozone may occur roughly a decade after the maximum chlorine abundance in the stratosphere, and roughly 15 years after the decline in the emission of CFCs (recently observed in the troposphere for some compounds[30]). Thus recovery of the Earth's ozone layer may take place later than currently expected. □

Received 14 July 1997; accepted 10 February 1998.

1. *Scientific Assessment of Ozone Depletion: 1994* (Rep. 37, World Meteorological Organization, Geneva, 1995).
2. Fels, S. B., Mahlman, J. D., Schwarzkopf, M. D. & Sinclair, R. W. Stratospheric sensitivity to perturbations in ozone and carbon dioxide: radiative and dynamical response. *J. Atmos. Sci.* **37,** 2265–2297 (1980).
3. Rind, D., Suozzo, R., Balachandran, N. K. & Prather, M. J. Climate change and the middle atmosphere. Part I: the doubled CO_2 climate. *J. Atmos. Sci.* **47,** 475–494 (1990).
4. Rind, D., Shindell, D. T., Lonergan, P. & Balachandran, N. K. Climate change and the middle atmosphere. Part III: the doubled CO_2 climate revisited. *J. Clim.* (in the press).
5. Mahfouf, J. F., Cariolle, D., Royer, J.-F., Geleyn, J.-F. & Timbal, B. Response of the Météo-France climate model to changes in CO_2 and sea surface temperature. *Clim. Dyn.* **9,** 345–362 (1994).
6. Manney, G. L., Santee, M. L., Froidevaux, L., Waters, J. W. & Zurek, R. W. Polar vortex conditions during the 1995–96 Arctic winter: Meteorology and MLS ozone. *Geophys. Res. Lett.* **23,** 3203–3206 (1996).
7. Müller, R. *et al.* Severe chemical ozone loss during the Arctic winter of 1995–96. *Nature* **389,** 709–712 (1997).
8. Rex, M. *et al.* Prolonged stratospheric ozone loss in the 1995–96 Arctic winter. *Nature* **389,** 835–838 (1997).
9. Newman, P. A., Gleason, J. F., McPeters, R. D. & Stolarski, R. S. Anomalously low ozone over the Arctic. *Geophys. Res. Lett.* **24,** 2689–2692 (1997).
10. Rind, D. *et al.* The GISS global climate/middle atmosphere model. Part I: model structure and climatology. *J. Atmos. Sci.* **45,** 329–370 (1988).
11. Shindell, D. T., Wong, S. & Rind, D. Interannual variability of the Antarctic ozone hole in a GCM. Part 1: the influence of tropospheric wave variability. *J. Atmos. Sci.* **54,** 2308–2319 (1997).
12. von Clarmann, T. *et al.* Determination of the stratospheric chlorine budget in the spring arctic vortex from MIPAS B limb emission spectra and air sampling experiments. *J. Geophys. Res.* **100,** 13979–13997 (1995).
13. Woodbridge, E. L. *et al.* Estimates of total organic and inorganic chlorine in the lower stratosphere from in situ and flask measurements during AASE II. *J. Geophys. Res.* **100,** 3057–3064 (1995).
14. Shindell, D. T., Rind, D. & Lonergan, P. Climate change and the middle atmosphere. Part IV: ozone response to doubled CO_2. *J. Clim.* (in the press).
15. Shindell, D. T. & de Zafra, R. L. Limits on heterogeneous processing in the Antarctic spring vortex from a comparison of measured and modelled chlorine. *J. Geophys. Res.* **102,** 1441–1449 (1997).
16. Jaeglé, L. *et al.* Evolution and stoichiometry of heterogeneous processing in the Antarctic stratosphere. *J. Geophys. Res.* **102,** 13235–13253 (1997).
17. Shindell, D. T. & de Zafra, R. L. Chlorine monoxide in the Antarctic spring vortex 2. A comparison of measured and modelled diurnal cycling over McMurdo Station, 1993. *J. Geophys. Res.* **101,** 1475–1487 (1996).
18. Santee, M. L., Manney, G. L., Read, W. G., Froidevaux, L. & Walters, J. W. Polar vortex conditions during the 1995–96 Arctic winter: MLS ClO and HNO_3. *Geophys. Res. Lett.* **23,** 3207–3210 (1996).
19. Pitari, G., Palermi, S., Visconti, G. & Prinn, R. G. Ozone response to a CO_2 doubling: results from a stratospheric circulation model with heterogeneous chemistry. *J. Geophys. Res.* **97,** 5953–5962 (1992).
20. Cariolle, D., Lasserre-Bogorry, A., Royer, J. F. & Geleyn, J. F. A general circulation model simulation of the springtime Antarctic ozone decrease and its impact on mid-latitutes. *J. Geophys. Res.* **95,** 1883–1898 (1990).
21. Mahlman, J. D., Pinto, J. P. & Umscheid, L. J. Transport, radiative, and dynamical effects of the Antarctic ozone hole: A GFDL "SKYHI" model experiment. *J. Atmos. Sci.* **51,** 489–508 (1994).
22. Austin, J., Butchart, N. & Shine, K. Possibility of an Arctic ozone hole in a doubled-CO_2 climate. *Nature* **360,** 221–225 (1992).
23. Austin, J. & Butchart, N. The influence of climate change and the timing of stratospheric warmings on Arctic ozone depletion. *J. Geophys. Res.* **99,** 1127–1145 (1994).
24. O'Neill, A. & Pope, V. D. Simulation of linear and non-linear disturbances in the stratosphere. *Q. J. R. Meteorol. Sci.* **114,** 1063–1075 (1988).
25. Houghton, J. T., Callander, B. A. & Varney, S. K. (eds) *Climate Change 1992; The Supplementary Report to the IPCC Scientific Assessment* (Cambridge Univ. Press, 1992).
26. Pawson, S. & Naujokat, B. Trends in daily wintertime temperatures in the northern stratosphere. *Geophys. Res. Lett.* **24,** 575–578 (1997).
27. Kodera, K. & Koide, H. Spatial and seasonal characteristics of recent decadal trends in the northern hemispheric troposphere and stratosphere. *J. Geophys. Res.* **102,** 19433–19447 (1997).
28. Zurek, R. W., Manney, G. L., Miller, A. J., Gelman, M. E. & Nagatani, R. M. Interannual variability of the north polar vortex in the lower stratosphere during the UARS mission. *Geophys. Res. Lett.* **23,** 289–292 (1996).
29. Farman, J. C., Gardiner, B. G. & Shanklin, J. D. Large losses of total ozone in Antarctica reveal seasonal ClOx/NOx interaction. *Nature* **315,** 207–210 (1985).
30. Montzka, S. A. *et al.* Decline in the tropospheric abundance of halogen from halocarbons: Implications for stratospheric ozone depletion. *Science* **272,** 1318–1322 (1996).

Acknowledgements. We thank J. Hansen, R. de Zafra, G. Schmidt and J. Knox for comments. This work was supported by the NASA Atmospheric Chemistry Modeling and Analysis Program and the NASA Climate Modeling Program.

Correspondence and requests for materials should be addressed to D.T.S. (e-mail: dshindell@giss.nasa.gov).

Variability of the path of the Kuroshio ocean current over the past 25,000 years

Ken Sawada*† & Nobuhiko Handa*†

** Institute for Hydrospheric-Atmospheric Sciences, Nagoya University, Chikusa-ku, Nagoya 464-01, Japan*

The Kuroshio current is the strong northwestern component of the subtropical North Pacific Ocean gyre, and advects a large amount of heat from the tropics to northern mid-latitudes. The Kuroshio has bimodal stationary flow patterns, with small and large meander paths east of central Japan[1,2] which switch on annual and decadal timescales[3,4]. These switches seem to be caused by changes in current velocity and volume transport of the North Equatorial Current that are associated with variations in the trade-wind intensity in the eastern equatorial North Pacific Ocean[5,6]. Here we present alkenone-derived sea surface temperature records at multicentennial resolution from sediment cores from the Nishishichitou ridge off central Japan. These 25,000-year records show that the Kuroshio path has also fluctuated on millennial timescales. This variability resembles that of the subtropical high pressure of the North Pacific, reconstructed from terrestrial pollen distributions, water levels in North American lakes, and marine micropalaeontological records[7]. Together, these data indicate that climate variability off central Japan over the past 25,000 years may be part of a circum-Pacific phenomenon, reflecting the rate of subtropical surface circulation in the North Pacific Ocean.

Piston cores were collected from three locations (KT92-17 stations 14, 19 and 20) on the Nishishichitou ridge off central Japan, to reconstruct climate change in the northwestern North Pacific (Fig. 1). The surface hydrographic conditions around the ridge are controlled largely by latitudinal migration of the current axis of the Kuroshio, known as its small and large meander paths (Fig. 1). With the small meander path, a warm water mass derived from the Kuroshio occupies the surface layer around station 14. Thus, water temperatures around this station have often been significantly higher than those to the south, creating a counter-current of the Kuroshio with a geostrophic balance around stations 19 and 20 (ref. 8). With the large meander path, a large cold surface water mass is established off central Japan which lowers sea surface temperatures (SST) around station 14. These two flow patterns are both stable, and alternate over short timescales[3,4].

The unsaturation ratio of C_{37} alkenones ($U^{k'}_{37}$; see definition[9] in

† Present addresses: Department of Chemistry, University of Tsukuba, Tsukuba, Ibaraki 305, Japan (K.S.); Aichi Prefectural University, Takada 3-28, Mizuho-ku, Nagoya 467, Japan (N.H.).